Jpn. J. Appl. Phys. Vol. 38 (1999) pp. 1403–1407
Part 1, No. 3A, March 1999

Electron Energy-Loss Spectroscopy Study of the Metal-Insulator Transition in $(V_{1-x}Cr_x)_2O_3$ ($x = 0.012$)

Hiroyuki ABE*, Masami TERAUCHI, Michiyoshi TANAKA and Shik SHIN[1]
Research Institute for Scientific Measurements, Tohoku University, Sendai 980-8577, Japan
[1]*Synchrotron Radiation Laboratory, Institute for Solid State Physics, The University of Tokyo, Tokyo 188-0002, Japan*

(Received October 14, 1998; accepted for publication December 22, 1998)

Electron energy-loss spectra of $(V_{1-x}Cr_x)_2O_3$ ($x = 0.012$) at the antiferromagnetic insulating (AFI), paramagnetic metallic (PM) and paramagnetic insulating (PI) phases have been measured using a high-resolution transmission electron energy-loss spectroscopy (EELS) microscope. The changes in the EELS spectra at the transition from the PM phase to the AFI phase are interpreted in a similar manner to the case of V_2O_3 [Jpn. J. Appl. Phys. **37** (1998) 584]. The change in the electronic structure at the transition from the PM phase to the PI phase (Mott transition) was revealed for the first time. A sharp peak observed at 1.0 eV in the PM phase did not appear in the PI phase. The t_{2g} peak of the O $1s \rightarrow$ V $3d(t_{2g})$ EELS spectra shows an energy increase of 0.5 eV at the transition from the PM phase to the PI phase. This increase is interpreted to occur by the splitting of the bonding e_g^π band, which is partially filled in the PM phase, into the fully occupied lower band and the unoccupied upper band, and by the lifting of the unoccupied band to an energy higher than the Fermi level in the PM phase. The t_{2g} peak also shows a decrease in intensity but an increase in the full width at half-maximum (FWHM) at the transition. The decrease in intensity occurs due to the decrease of the hybridization of the V $3d$ with the O $2p$ orbitals resulting from an increase of the V–O distance. The increase in the FWHM results from the lifting of the a_{1g}^* band due to the decrease of the lattice constant c_H and the splitting of the e_g^π and $e_g^{\pi *}$ bands each into two bands due to electron correlation.

KEYWORDS: metal-insulator transition, EELS, free-carrier plasmon, interband transition, interband plasmon, unoccupied density of states

1. Introduction

In previous papers, we have showed the changes in the electronic structures of VO_2 and V_2O_3 at the metal-insulator transition (MIT) using the high-resolution transmission electron energy-loss spectroscopy (EELS) technique.[1,2] In the case of V_2O_3, a sharp peak was observed at about 1 eV in the EELS spectrum of the paramagnetic metallic (PM) phase but not in that of the antiferromagnetic insulating (AFI) phase. An edge structure at about 1 eV observed in optical reflectivity has been assigned to the plasma edge.[3] We, however, assigned the peak to an interband plasmon caused by d–d transitions, based on the inspection of the dielectric function derived from the loss function.[2] The peak due to the O $1s \rightarrow$ V $3d(t_{2g})$ transition in the O $1s$ EELS spectra increased in energy by 0.4 eV but decreased in intensity at the transition from the PM phase to the AFI phase. The increase of the energy is interpreted to occur due to the splitting of the V $3d(t_{2g})$ band, which is partially filled in the PM phase, into the fully occupied and unoccupied bands, and by the lifting of the unoccupied band to a state with an energy higher than the Fermi level in the PM phase. The decrease in intensity is considered to be due to the decrease of the transition probability of the O $1s \rightarrow$ V $3d(t_{2g})$ transition, which is attributed to the decrease of the hybridization of V $3d$ with O $2p$ orbitals at the transition from the PM phase to the AFI phase.[2]

Vanadium sesquioxide (V_2O_3) undergoes an MIT with a change of temperature,[4] which is accompanied by changes in the crystal[5] and magnetic[6] structures. It has the corundum structure with space group $R\bar{3}c$ in the PM phase above 150 K and a monoclinic structure with space group $B2/b$ in the AFI phase below 150 K. Feinleib and Paul[7] reported that the resistivity of V_2O_3 increases gradually above 400 K. Since this transition suffers no changes in the crystal and magnetic structures, though lattice constants change continuously, it appears to be a Mott transition, which results from the localization of electrons.[8]

According to Goodenough,[9] the fivefold degenerate V $3d$ levels split into triply degenerate lower t_{2g} levels and doubly degenerate upper e_g levels due to the cubic component of the octahedral crystal field. One of the t_{2g} orbitals (a_{1g} orbital), which extends toward the orbitals of the nearest-neighbor vanadium atoms, forms the a_{1g} band. The other two t_{2g} orbitals (e_g^π orbitals), which extend toward the orbitals of the second nearest-neighbor vanadium atoms, form the e_g^π band. Both the a_{1g} band and the e_g^π band split into the bonding band and the antibonding band. These two a_{1g} and e_g^π bands almost overlap. The metallic behavior above 150 K is caused by the partial filling of the overlapping bands with two $3d$ electrons per vanadium ion [Fig. 1(a)]. Goodenough[9] explained the transition from the PM phase to the AFI phase as follows. When V_2O_3 undergoes the monoclinic distortion below 150K, the e_g^π band splits into the [010] band, which extends to the [010] direction of the phase, and the (010) band, which extends on the (010) plane. The $[a_{1g} + (010)]$ band, which is formed by the overlapping of the a_{1g} band and the (010) band, splits into the $[a_{1g}+(010)]\alpha$ band and the $[a_{1g}+(010)]\beta$ band due to an interatomic exchange interaction. These two bands are separated from each other by an interatomic exchange energy (Δ_{ex}). The insulating behavior below 150 K is caused by the complete filling of the [010] bonding band and the $[a_{1g} + (010)]\alpha$ bonding band [Fig. 1(b)]. The transition from the PM phase to the PI phase is explained as follows, though Goodenough[9] did not explain it in ref. 9. The lattice constant c_H slightly decreases but a_H slightly increases with an increase in temperature.[8] Since the decrease of c_H increases the hybridization of the a_{1g} orbitals, the energy difference between the a_{1g} bonding band and the a_{1g} antibonding band increases. Since the increase of a_H decreases the hybridization

*Present address: Department of Materials Science, Japan Atomic Energy Research Institute, Tokai-mura, Ibaraki 319-1195, Japan

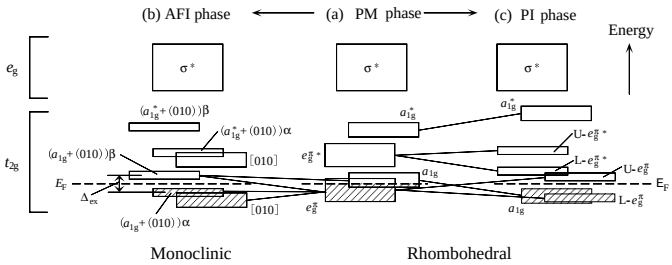

Fig. 1. Schematic band diagram of V_2O_3 at the PM (a), AFI (b) and PI (c) phases. The asterisk indicates antibonding. U and L mean upper and lower, respectively.

of the e_g^π orbitals, the energy difference between the e_g^π bonding band and the e_g^π antibonding band decreases. The transition to an insulator or the PI phase was considered to be caused by the splitting of the e_g^π bonding band into the lower and upper e_g^π bonding bands (Mott-Hubbard splitting)[10] and by the complete filling of the a_{1g} bonding band and the lower e_g^π bonding band [Fig. 1(c)].

Spectra measurements of V_2O_3 at room temperature and high temperatures of about 800 K are necessary to reveal the changes of the electronic structure at the Mott transition. Unfortunately, it is difficult to obtain reliable spectra of the paramagnetic insulating (PI) phase because oxygen deficiencies are induced at high temperatures. McWhan and Remeika[8] showed that the resistivity suddenly increases at a temperature between 200–300 K and the transition temperature is lowered to this temperature by 1% doping of Cr. Kuwamoto *et al.*[11] measured the resistivity of the $(V_{1-x}Cr_x)_2O_3$ system ($0 \leq x \leq 0.1$) and showed that the samples of $0.0051 \leq x \leq 0.0178$ undergo the transition from the PI phase to the PM phase at 200–380 K and the transition from the PM phase to the AFI phase at 160–184 K. Thus, the change of the electronic structure at the Mott transition can be more easily investigated when a few percent of Cr is doped in V_2O_3. It is considered that the MITs in the $(V_{1-x}Cr_x)_2O_3$ system are caused by the same mechanism as those in V_2O_3 described above.

Changes in electronic structures of the $(V_{1-x}Cr_x)_2O_3$ system at the MITs were studied by optical spectroscopy,[12,13] ultraviolet photoelectron spectroscopy (UPS) and X-ray photoelectron spectroscopy (XPS).[14,15] Barker and Remeika[12] showed optical conductivity of $(V_{1-x}Cr_x)_2O_3$ ($x = 0.012$) at the AFI, PM and PI phases over an energy range of 0.04–3 eV. They reported that the band-gap energies of the AFI and PI phases are approximately 0.1 and 0.1–0.5 eV, respectively. However, they did not show the changes of the dielectric functions at the MITs. Smith and Henrich[14] measured UPS and XPS spectra of $(V_{1-x}Cr_x)_2O_3$ ($x = 0.015$) at the AFI, PM and PI phases. They showed the changes in the occupied density of states (DOS) near the Fermi level at the MITs. Unfortunately, the changes in the unoccupied DOS at the MITs have never been studied.

We have measured the EELS spectra of $(V_{1-x}Cr_x)_2O_3$ ($x = 0.012$) in valence and core electron excitation regions for the first time to reveal the changes in electronic structures at the MITs, especially at the transition from the PM phase to the PI phase (Mott transition). The change of the EELS spectra at the valence electron excitation region is discussed using the dielectric function derived from the EELS spectra. The change in the EELS spectra at the core electron excitation region is explained in terms of the band structure.

2. Experimental

The high-resolution EELS microscope used was developed as a project of the Joint Research with Industry by the Ministry of Education, Science, Sports and Culture.[16,17] The EELS microscope is equipped with a thermal-type field emission gun as the electron source and specially designed stigmatic-focus Wien filters as the monochromator and the analyzer. The EELS microscope incorporates an illumination lens system, a specimen goniometer and an imaging lens system of a JEM1200EX transmission electron microscope. EELS spectra were taken by a parallel-recording system using a charge-coupled device (CCD) camera. The best values of the full width at half-maximum (FWHM) of the zero-loss peak are 12 meV without a specimen and 25 meV with a specimen. The incident electron energy was always set at 60 keV. The retarding potential of the monochromator was set to be 51 V and that of the analyzer was 200–520 V in this experiment.

Specimens for electron energy-loss spectra were prepared by crushing single crystals and placing the fragments on a mesh for electron microscopy. Electron energy-loss spectra were obtained from specimen areas of 180 nm in diameter. The specimen areas were judged to be perfectly crystalline from their good electron diffraction patterns. The maximum acceptance angle for inelastically scattered electrons was 2.5 mrad for the valence electron excitation spectra and 12 mrad for the core electron excitation spectra, which correspond to the momentum transfer of 3 and 15 nm^{-1}, respectively, at an incident electron energy of 60 keV. From the resistivity measurement,[18] $(V_{1-x}Cr_x)_2O_3$ ($x = 0.012$) used in the present study underwent the transition from the PI phase to the PM phase at 230 K and from the PM phase to the AFI phase at 170 K when the sample was cooled. The specimens were cooled in a cooling holder for electron microscopy. The temperature of the specimens was measured using a thermocouple near the specimens.

3. Results and Discussion

3.1 EELS spectra of the valence electron excitation region

Figure 2 shows EELS spectra of $(V_{1-x}Cr_x)_2O_3$ ($x = 0.012$) measured at the AFI (100 K), PM (200 K) and PI (300 K) phases over an energy range of 0–60 eV with energy resolutions of 93, 110 and 97 meV for the FWHM of the zero-loss peak, respectively. The EELS spectra of the AFI and PM phases were nearly the same as those of V_2O_3.[2] The small peak at about 5 eV and the sharp peak at about 12 eV are assigned to the interband transitions from the O $2p$ band to the V $3d$ band.[19] The peak at about 16 eV is assigned to the interband transitions from the O $2p$ band to the V $4s$, $4p$ band.[19] The large peak at about 26 eV is due to the collective excitation of all valence electrons (volume plasmon). The calculated plasmon energy using the Drude model is about 20 eV, which does not agree with the experimental value. The plasmon energy ($\hbar\omega_p$), however, is calculated more accurately by the Lorentz model using

$$\hbar\omega_p = \sqrt{(\hbar\omega_p^{(f)})^2 + (\hbar\omega_0)^2}, \tag{3.1}$$

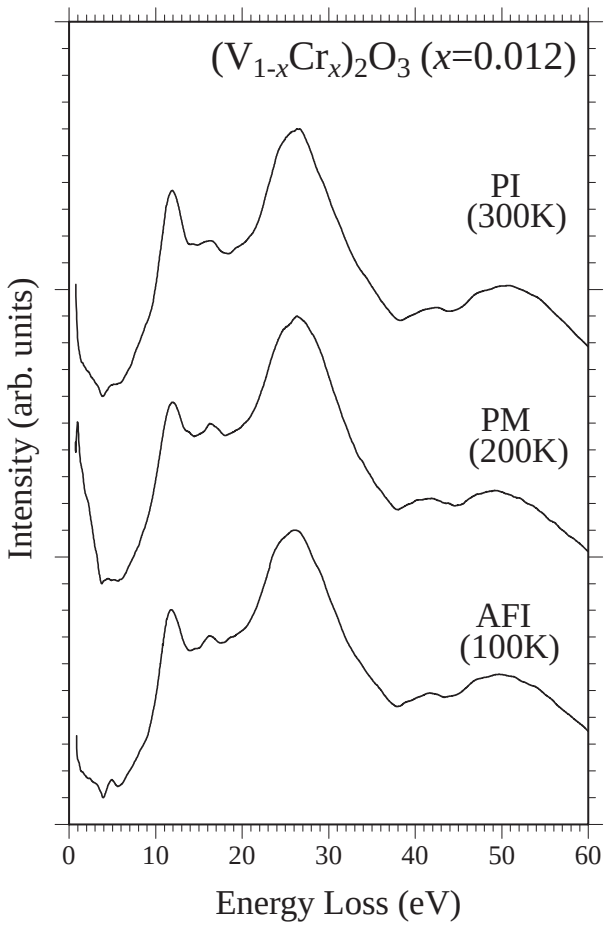

Fig. 2. Valence electron excitation spectra of $(V_{1-x}Cr_x)_2O_3$ ($x = 0.012$) measured at the AFI (100 K), PM (200 K) and PI (300 K) phases over an energy range of 0–60 eV with energy resolutions of 93, 110 and 97 meV, respectively.

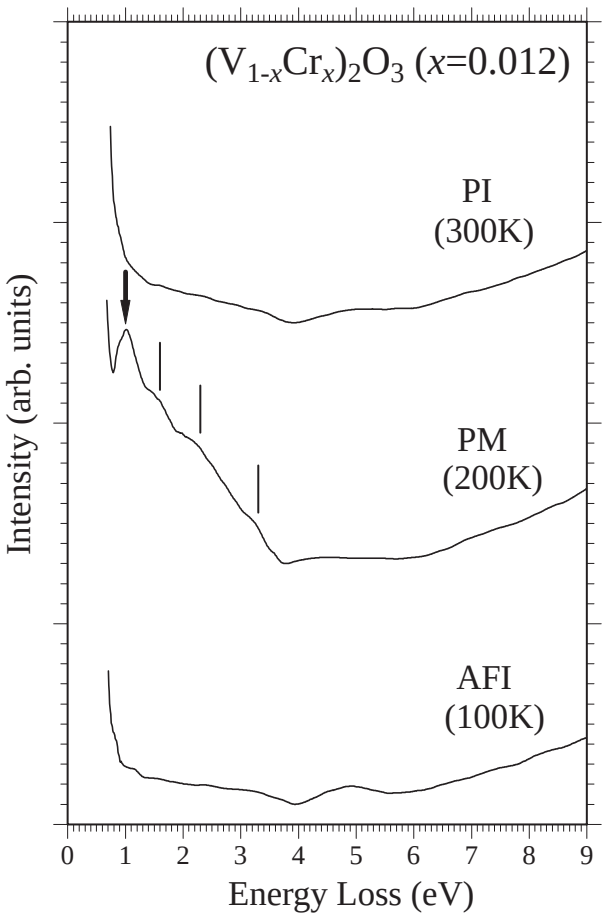

Fig. 3. Valence electron excitation spectra of $(V_{1-x}Cr_x)_2O_3$ ($x = 0.012$) measured at the AFI (100 K), PM (200 K) and PI (300 K) phases over an energy range of 0–9 eV with energy resolutions of 65, 74 and 59 meV, respectively. The peak at 1.0 eV indicated by an arrow disappeared at the transition from the PM phase to the PI phase.

where $\hbar\omega_p^{(f)}$ is the plasmon energy calculated from the Drude model and $\hbar\omega_0$ is the interband transition energy. Substituting $\hbar\omega_p^{(f)} = 20$ eV and $\hbar\omega_0 = 16$ eV, which is the closest interband transition energy to the volume plasmon energy, into eq. (3.1), we obtain $\hbar\omega_p = 26$ eV, which agrees well with the experimental value of 26 eV. The peak at about 42 eV and the shoulder at about 47 eV are assigned to the transitions from the V 3*p* core levels to the V 3*d* band, by referring to XPS spectra of V_2O_3.[15] The broad peak at around 50 eV is attributed to the double loss of the volume plasmon.

Figure 3 shows EELS spectra of $(V_{1-x}Cr_x)_2O_3$ ($x = 0.012$) measured at the AFI (100 K), PM (200 K) and PI (300 K) phases over an energy range of 0–9 eV with energy resolutions of 65, 74 and 59 meV for the FWHM of the zero-loss peak, respectively. The EELS spectra of the AFI and PM phases of $(V_{1-x}Cr_x)_2O_3$ ($x = 0.012$) are very similar to those of V_2O_3.[2] The peak at 1.0 eV, indicated by an arrow, disappears at the transition from the PM phase to the PI phase. The broad peak starting at about 4 eV is assigned to the interband transition from the O 2*p* band to the V 3*d* band. The peak increased in intensity at the transition from the PM phase to the PI phase. The change of this peak is considered to be due to the change of the unoccupied V 3*d* band because the UPS spectra showed that the occupied DOS of the O 2*p* band change negligibly at the MIT.[14]

The upper panels of Figs. 4(a), 4(b) and 4(c) show the loss function ($\mathrm{Im}[-1/\varepsilon(\omega)]$) of the AFI (100 K), PM (200 K) and PI (300 K) phases, respectively, derived from Figs. 2 and 3. The contributions of the direct beam and multiple scattering were removed by a Lorentz fit and the Fourier-log deconvolution method,[20] respectively. The absolute value of the loss function at the PM phase was determined by applying $\mathrm{Re}[-1/\varepsilon(0)] = 0$.[20] Since the refractive indices of the AFI and PI phases are not known, the absolute values of the loss functions at these phases were determined using the sum rule,[20]

$$\int_0^\infty \omega\,\mathrm{Im}\left[-\frac{1}{\varepsilon(\omega)}\right]d\omega = \frac{\pi}{2}(\omega_p^{(f)})^2, \tag{3.2}$$

$$\omega_p^{(f)} = (Ne^2/\epsilon_0 m)^{1/2}, \tag{3.3}$$

where ϵ_0 is the dielectric permittivity of vacuum, N is the density of all valence electrons, e is the electron charge and m is the mass of an electron. The dielectric function was calculated from the loss function and $\mathrm{Re}[1/\varepsilon(\omega)]$, which was derived from the loss function by Kramers-Kronig analysis. The integration with energy was carried out up to 400 eV in the three processes of Fourier-log deconvolution, determination of the absolute value of the loss function and Kramers-Kronig analysis, where the loss function above 60 eV was obtained by extrapolating the loss function using E^{-4} dependence.[1,2,21] The lower panels of Figs. 4(a), 4(b) and 4(c) show the real

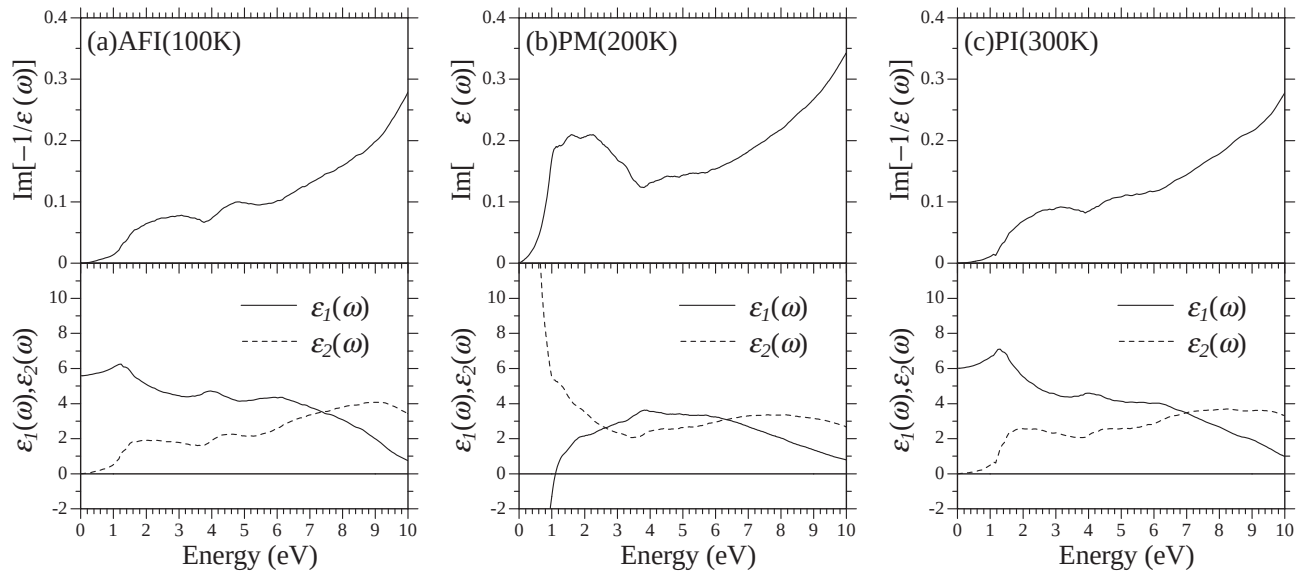

Fig. 4. The loss function (Im[$-1/\varepsilon(\omega)$]), the real part (ε_1) and the imaginary part (ε_2) of the dielectric function of $(V_{1-x}Cr_x)_2O_3$ ($x = 0.012$) at the AFI (100 K) (a), PM (200 K) (b) and PI (300 K) (c)phases. The dielectric function was derived by Kramers-Kronig analysis of the loss function.

(ε_1) and imaginary (ε_2) parts of the dielectric function of the AFI (100 K), PM (200 K) and PI (300 K) phases, respectively. The dielectric functions of the AFI [Fig. 4(a)] and PM [Fig. 4(b)] phases of $(V_{1-x}Cr_x)_2O_3$ ($x = 0.012$) are very similar to those of V_2O_3.[2)] Since the condition for the plasmon excitation ($\varepsilon_1 = 0$) is satisfied at 1.1 eV in the PM phase [Fig. 4(b)], the peak at 1.0 eV in the loss function of the PM phase is assigned to a plasmon excitation. However, the free-carrier plasmon is expected to be observed at 7.3 eV, which is calculated from eq. (3.3) using the carrier density of V_2O_3 at the PM phase of 3.85×10^{28} m^{-3}.[22)] ε_2 shows peaks and shoulders (interband transition character) around 1.1 eV, which are assigned to d–d transitions by the same reason as in the case of V_2O_3.[2)] Thus, the peak at 1.0 eV in the loss function is assigned to an interband plasmon peak. The dielectric function of the PI phase [Fig. 4(c)] was obtained for the first time in the present study. The ε_1 and ε_2 curves in the low-energy region show the behavior of an insulator, as expected from the measurement of the conductivity.[11)] Nonexistence of the plasmon excitation condition is also reflected by the behavior of the dielectric function.

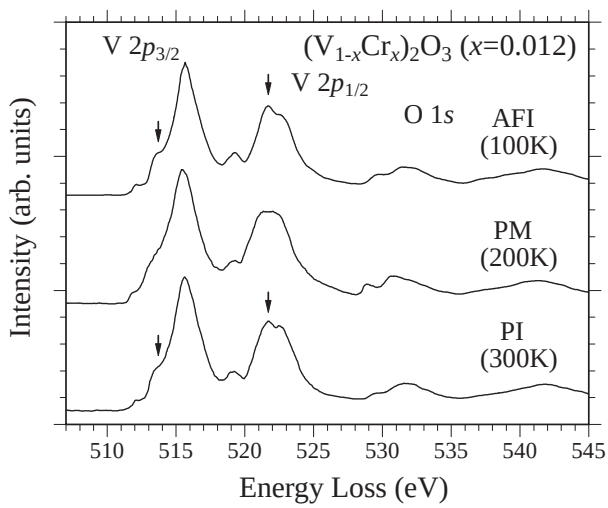

Fig. 5. V 2p and O 1s core electron excitation spectra of $(V_{1-x}Cr_x)_2O_3$ ($x = 0.012$) measured at the AFI (100 K), PM (200 K) and PI (300 K) phases over an energy range of 507–545 eV with an energy resolution of 0.21 eV.

3.2 EELS spectra of the core electron excitation region

Figure 5 shows EELS spectra of $(V_{1-x}Cr_x)_2O_3$ ($x = 0.012$) measured at the AFI (100 K), PM (200 K) and PI (300 K) phases over an energy range of 507–545 eV with an energy resolution of 0.21 eV, which was determined by the FWHM of the zero-loss peak. The spectra below 527 eV are the V 2p EELS spectra and those above 527 eV are the O 1s EELS spectra. The peaks at about 516 and 522 eV are attributed to excitations from the V $2p_{3/2}$ and V $2p_{1/2}$ core levels, respectively. The experimental spectral intensity ratio of the V $2p_{3/2}$ to V $2p_{1/2}$ excitations is different from that expected from spin-orbit splitting (2 : 1). This is because a strong core-hole interaction exists between the hole in the V 2p core level and the electron excited into the unoccupied V 3d band from the core level.[23)] The peak energy of the V 2p EELS spectrum showed little difference among the PI, PM and AFI phases. The peaks at 513.7 and 521.7 eV, indicated by arrows in the spectra of the AFI and PI phases, are sharper than those of the PM phase. This difference should be due to MITs but cannot be explained simply due to the strong core hole interaction. Theoretical calculations are needed to quantitatively explain the V 2p EELS spectra.

On the other hand, the core-hole interaction between the electron excited into the unoccupied V 3d band from the O 1s core level and the hole is weak. Thus, the change of the unoccupied V 3d band at the MIT can be directly related to the change of the O 1s EELS spectra. Figure 6 shows the O 1s EELS spectra measured at the AFI (100 K), PM (200 K) and PI (300 K) phases. The peaks at about 529 and 532 eV are assigned to the transitions from the O 1s core level to the unoccupied V $3d(t_{2g})$ and V $3d(e_g)$ bands, respectively. These transitions are possible through an admixture of the V 3d orbitals with the O 2p orbitals, though they are not allowed by

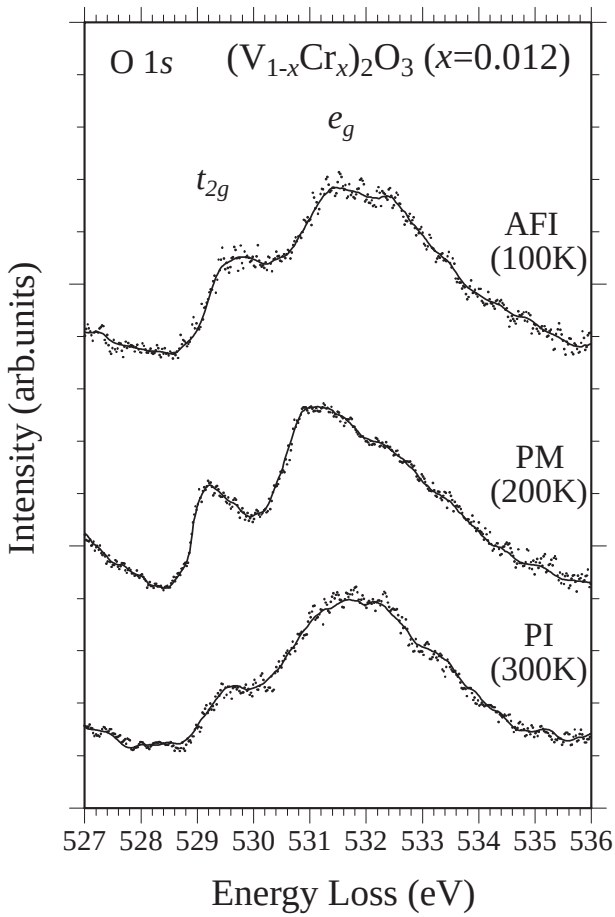

Fig. 6. O 1*s* core electron excitation spectra of $(V_{1-x}Cr_x)_2O_3$ ($x = 0.012$) measured at the AFI (100 K), PM (200 K) and PI (300 K) phases.

the dipole transition. The t_{2g} peak of the O $1s \rightarrow$ V $3d(t_{2g})$ EELS spectra shows an energy increase of 0.5 eV at the transition from the PM phase to the PI phase. This increase is interpreted to occur due to the splitting of the bonding e_g^{π} band, which is partially filled at the PM phase, into the fully occupied lower band and the unoccupied upper band, and the lifting of the unoccupied band to an energy higher than the Fermi level in the PM phase. The t_{2g} peak has also shows a decrease in intensity but an increase in the FWHM at the transition. The decrease in intensity occurs because of the decrease of the hybridization of the V $3d$ with the O $2p$ orbitals due to an increase in the V–O distance. [5] The increase in the FWHM is a result of the lifting of the a_{1g}^{*} band due to the decrease of the lattice constant c_H and the splitting of the e_g^{π} and $e_g^{\pi *}$ bands each into two bands due to electron correlation [Fig. 1(c)]. We revealed the change of the unoccupied DOS of the V $3d$ band from the change of the O $1s$ EELS spectra at the MIT.

4. Concluding Remarks

We measured the EELS spectra of Cr-doped V_2O_3 at the AFI, PM and PI phases. The changes of the EELS spectra at the transition from the PM phase to the AFI phase were interpreted in a similar manner to the case of V_2O_3.[2] The change of the EELS spectra at the transition from the PM phase to the PI phase (Mott transition) was revealed for the first time using Cr-doped V_2O_3 instead of V_2O_3. The change in the EELS spectra of the valence electron excitation region at the transition from the PM phase to the PI phase was discussed using the dielectric function derived from the EELS spectra. The change in the O $1s$ EELS spectra at the transition was explained in terms of the band structure.

It is expected that theoretical V $2p$ EELS spectra will be calculated to quantitatively explain the change of the experimental EELS spectra. The mixed-valence compound V_6O_{13} also undergoes the MIT with the change of temperature.[24] The EELS study of V_6O_{13} will be reported elsewhere.

Acknowledgements

The authors would like to thank Mr. F. Sato for his skillful technical assistance. The present work was partly supported by a Grant-in-Aid from the Ministry of Education, Science, Sports and Culture.

1) H. Abe, M. Terauchi, M. Tanaka, S. Shin and Y. Ueda: Jpn. J. Appl. Phys. **36** (1997) 165.
2) H. Abe, M. Terauchi, M. Tanaka and S. Shin: Jpn. J. Appl. Phys. **37** (1998) 584.
3) S. Stizza, I. Davoli, R. Bernardini, A. Bianconi and M. Benfatto: Solid State Commun. **48** (1983) 471.
4) F. J. Morin: Phys. Rev. Lett. **3** (1959) 34.
5) P. D. Dernier and M. Marezio: Phys. Rev. B **2** (1970) 3771.
6) R. M. Moon: Phys. Rev. Lett. **25** (1970) 527.
7) J. Feinleib and W. Paul: Phys. Rev. **155** (1967) 841.
8) D. B. McWhan and J. P. Remeika: Phys. Rev. B **2** (1970) 3734.
9) J. B. Goodenough: Proc. 10th Int. Conf. Physics of Semiconductors, Boston, 1970 p. 304.
10) C. Tatsuyama and S. Ichimura: Kotai Buturi **16** (1981) 189 [in Japanese].
11) H. Kuwamoto, J. M. Honig and J. Appel: Phys. Rev. B **22** (1980) 2626.
12) A. S. Barker Jr. and J. P. Remeika: Solid State Commun. **8** (1970) 1521.
13) E. D. Isaacs, P. M. Platzman, P. Metcalf and J. M. Honig: Phys. Rev. Lett. **76** (1996) 4211.
14) K. E. Smith and V. E. Henrich: Phys. Rev. B **50** (1994) 1382.
15) S. Shin, Y. Tezuka, T. Kinoshita, A. Kakizaki, T. Ishii, Y. Ueda, W. Jang, H. Takei, Y. Chiba and M. Ishigame: Phys. Rev. B **46** (1992) 9224.
16) M. Terauchi, R. Kuzuo, F. Satoh, M. Tanaka, K. Tsuno and J. Ohyama: Microsc. Microanal. Microstruct. **2** (1991) 351.
17) M. Tanaka, M. Terauchi, R. Kuzuo, K. Tsuno, J. Ohyama and Y. Harada: *Proc. 50th Annu. Meet. Electron Microscopy Society of America*, eds. G. W. Beily, J. Bentley and J. A. Small (San Francisco Press, San Francisco, 1992) p. 940.
18) S. Shin: private communication.
19) S. Shin, S. Suga, M. Taniguchi, M. Fujiwara, H. Kanazaki, A. Fujimori, H. Daimon, Y. Ueda, K. Kosuge and S. Kachi: Phys. Rev. B **41** (1990) 4993.
20) R. F. Egerton: *Electron Energy Loss Spectroscopy in the Electron Microscope* (Plenum Press, New York and London, 1996).
21) M. Terauchi, M. Tanaka, T. Takahashi, H. Katayama-Yoshida, T. Mochiku and K. Kadowaki: Jpn. J. Appl. Phys. **34** (1995) L1524.
22) V. P. Zhuze, A.A. Andreev and A. I. Shelykh: Fiz. Tverd. Tela **10** (1968) 3674. Translation: Sov. Phys.–Solid State **10** (1968) 2914.
23) J. Zaanen, G. A. Sawatzky, J. Fink, W. Speier and J. C. Fuggle: Phys. Rev. B **32** (1985) 4905.
24) S. Kachi, T. Takada and K. Kosuge: J. Phys. Soc. Jpn. **18** (1963) 1839.